

Overlapping Resonances Interference-induced Transparency: The $S_0 \rightarrow S_2/S_1$ Photoexcitation Spectrum of Pyrazine

Timur Grinev

*Chemical Physics Theory Group, Department of Chemistry, and Center for Quantum Information and Quantum Control,
University of Toronto, Toronto, Ontario M5S 3H6, Canada*

Moshe Shapiro

*Department of Chemistry, University of British Columbia, Vancouver, British Columbia
V6T 1Z1, Canada, and Department of Chemical Physics, Weizmann Institute of Science, Rehovot 76100, Israel*

Paul Brumer

*Chemical Physics Theory Group, Department of Chemistry, and Center for Quantum Information and Quantum Control,
University of Toronto, Toronto, Ontario M5S 3H6, Canada*

The phenomenon of “overlapping resonances interference-induced transparency” (ORIT) is introduced and studied in detail for the $S_0 \rightarrow S_2/S_1$ photoexcitation of cold pyrazine ($C_4H_4N_2$). In ORIT a molecule becomes transparent at specific wavelengths due to interferences between envelopes of spectral lines displaying overlapping resonances. An example is the $S_2 \leftrightarrow S_1$ internal conversion in pyrazine where destructive interference between overlapping resonances causes the $S_0 \rightarrow S_2/S_1$ light absorption to disappear at certain wavelengths. ORIT may be of practical importance in multi-component mixtures where it would allow for the selective excitation of some molecules in preference to others. Interference induced cross section enhancement is also shown.

I. INTRODUCTION

In “Electromagnetically Induced Transparency” (EIT) [1–8], one creates a photoabsorption transparency window at certain frequencies by applying a (“coupling”) laser operating at another set of frequencies. In this paper we investigate a related, though distinct, physical phenomenon, called “overlapping resonances interference-induced transparency” (ORIT), where the transparency occurs due to interference between material waves within a molecule. Though ORIT is known for small systems [9, 10], it has not been investigated for polyatomic molecules where overlapping resonances are far more ubiquitous. In the present paper we introduce the ORIT phenomenon for polyatomic molecules, and examine it in detail in the $S_0 \rightarrow S_2/S_1$ photoabsorption of pyrazine ($C_4H_4N_2$).

II. THE PYRAZINE $S_0 \rightarrow S_2/S_1$ PHOTOEXCITATION

The ultrafast dynamics of pyrazine is of longstanding interest. For example, in recent work where the computational tools used in this paper were developed, we studied pyrazine $S_2 \leftrightarrow S_1$ internal conversion, using a pre-excited superposition state in S_2 as a starting point [11–14], or creating such superposition state in the $S_0 \rightarrow S_2/S_1$ ultrafast laser excitation [15, 16]. In the course of these prior studies [12] a detailed understanding of the vibronic structure and intramolecular dynamics of pyrazine was obtained.

We denote as intramolecular $|\kappa\rangle$ “resonances” the vibrational states of the noninteracting S_2 electronic state, and the projector onto this resonance manifold as $Q = \sum_{\kappa} |\kappa\rangle\langle\kappa|$. These resonances are coupled to the vibrational states of the S_1 electronic state, denoted as $|\beta\rangle$, with $P = \sum_{\beta} |\beta\rangle\langle\beta|$ being the projector onto the manifold of these states. When we ignore the coupling to the pyrazine triplet T states [17], the eigenstates of the excited $S_1 + S_2$ Hamiltonian, denoted as $|\gamma\rangle$, take into account the $S_1 \leftrightarrow S_2$ couplings. We thus have that $P + Q = I = \sum_{\gamma} |\gamma\rangle\langle\gamma|$ where I is the identity operator on the excited states manifold. Even in the neglect of rotations, the $S_0 \rightarrow S_2/S_1$ photoabsorption process becomes a formidable 24 modes vibrational problem.

We now examine conditions under which the (weak field) photoabsorption cross section $\sigma(E)$ given as [10, 18]

$$\sigma(E_{\gamma}) = \frac{4\pi^2\omega_{\gamma,g}}{c} |\langle\gamma|\mu|g\rangle|^2, \quad (1)$$

vanishes, where $|g\rangle$ is the ground vibrational state of S_0 , μ is the transition-dipole operator, and $\omega_{\gamma,g} \equiv (E_{\gamma} - E_g)/\hbar$ is the excitation frequency. For E_{γ} above the S_2 potential minimum, the full excited vibronic state $|\gamma\rangle$ is composed of both the S_2 and the S_1 vibrational states (remembering that the S_1 potential minimum lies below the S_2 potential minimum). It was previously established [11–13, 19] that $\langle\kappa|\mu|g\rangle$, the dipole matrix elements for the pure $S_0 \rightarrow S_2$ transitions, are an order of magnitude larger than $\langle\beta|\mu|g\rangle$, the analogous matrix elements for the pure $S_0 \rightarrow S_1$ transitions. Hence, one can introduce the so-called “doorway states” approximation, according to which,

$$\langle\gamma|\mu|g\rangle = \langle\gamma|(P + Q)\mu|g\rangle = \sum_{\beta} \langle\gamma|\beta\rangle\langle\beta|\mu|g\rangle + \sum_{\kappa} \langle\gamma|\kappa\rangle\langle\kappa|\mu|g\rangle \approx \sum_{\kappa} \langle\gamma|\kappa\rangle\langle\kappa|\mu|g\rangle. \quad (2)$$

This yields, for $\sigma(E_{\gamma})$:

$$\sigma(E_{\gamma}) = \frac{4\pi^2\omega_{\gamma,g}}{c} \left| \sum_{\kappa} \langle\gamma|\kappa\rangle\langle\kappa|\mu|g\rangle \right|^2. \quad (3)$$

The cross section in Eq. (3) can be expanded as

$$\sigma(E_{\gamma}) = \frac{4\pi^2\omega_{\gamma,g}}{c} \left[\sum_{\kappa} |\langle\gamma|\kappa\rangle\langle\kappa|\mu|g\rangle|^2 + \sum_{\kappa \neq \kappa'} \langle g|\mu|\kappa\rangle\langle\kappa'|\mu|g\rangle\langle\kappa|\gamma\rangle\langle\gamma|\kappa'\rangle \right]. \quad (4)$$

The first (positive) part of Eq. (4),

$$\sigma^{\text{diag}}(E_{\gamma}) = \sum_{\kappa} \frac{4\pi^2\omega_{\gamma,g}}{c} |\langle\gamma|\kappa\rangle\langle\kappa|\mu|g\rangle|^2 \equiv \sum_{\kappa} \sigma_{\kappa}^{\text{diag}}(E_{\gamma}), \quad (5)$$

is the diagonal contribution to $\sigma(E_\gamma)$, composed of individual contributions $\sigma_\kappa^{\text{diag}}(E_\gamma)$ from the $|\kappa\rangle$ resonances, while

$$\sigma^{\text{interf}}(E_\gamma) = \sum_{\kappa \neq \kappa'} \frac{4\pi^2 \omega_{\gamma,g}}{c} \langle g|\mu|\kappa\rangle \langle \kappa'|\mu|g\rangle \langle \kappa|\gamma\rangle \langle \gamma|\kappa'\rangle \equiv \sum_{\kappa \neq \kappa'} \sigma_{\kappa,\kappa'}^{\text{interf}}(E_\gamma) = \sum_{\kappa < \kappa'} 2 \sigma_{\kappa,\kappa'}^{\text{interf}}(E_\gamma) \quad (6)$$

is the (positive or negative) interference contribution to $\sigma(E_\gamma)$, composed of pairwise interference terms $\sigma_{\kappa,\kappa'}^{\text{interf}}(E_\gamma)$, $\kappa \neq \kappa'$ ($\sigma_{\kappa,\kappa'}^{\text{interf}}(E_\gamma)$ in Eq. (6) are assumed real). Each pairwise interference term $\sigma_{\kappa,\kappa'}^{\text{interf}}(E_\gamma)$ is proportional to the product $\langle \kappa|\gamma\rangle \langle \gamma|\kappa'\rangle$, which is non-zero only if both $\langle \kappa|\gamma\rangle$ and $\langle \gamma|\kappa'\rangle$ are non-zero. When this happens, the $|\kappa\rangle$ and $|\kappa'\rangle$ resonances are said to *overlap*. The overlap is due to the common contribution of the full state $|\gamma\rangle$ (Ref. [12, 16]). In other words, for the pairwise interference contribution $\sigma_{\kappa,\kappa'}^{\text{interf}}(E)$ between resonances $|\kappa\rangle$ and $|\kappa'\rangle$ to be non-zero at the particular energy $E = E_\gamma$, $|\kappa\rangle$ and $|\kappa'\rangle$ must overlap at this energy through one or more common states $|\gamma\rangle$.

The $\sigma(E_\gamma)$ cross section is closely related to the S_2 excited state population $P_{S_2}(t)$ [16], generated by CW pulse $\varepsilon(\omega) \approx \epsilon_a \delta(\omega - \omega_{\gamma,g})$ that excites only one state $|\gamma\rangle$. To obtain $P_{S_2}(t)$, consider the excited wave packet $|\Psi_a(t)\rangle$ on S_1 and S_2 , produced by the one-photon transition from S_0 in the framework of first-order perturbation theory. For the CW case $|\Psi_a(t)\rangle$ takes the form:

$$|\Psi_a(t)\rangle = \frac{i\epsilon_a}{\hbar} \exp(-iE_\gamma t/\hbar) |\gamma\rangle \langle \gamma| \left[\sum_{\kappa} \langle \kappa|\mu|g\rangle |\kappa\rangle \right]. \quad (7)$$

Taking into account Eq. (2), we see that the last sum of Eq. (7) is $\mu|g\rangle \equiv |\Psi^e\rangle$ – an excited wave packet on S_2 . Thus,

$$|\Psi_a(t)\rangle = (i\epsilon_a/\hbar) \exp(-iE_\gamma t/\hbar) |\gamma\rangle \langle \gamma| \mu|g\rangle = (i\epsilon_a/\hbar) \exp(-iE_\gamma t/\hbar) |\gamma\rangle \langle \gamma| \Psi^e, \quad (8)$$

a result proportional to the action of the single-state propagator $\exp(-iE_\gamma t/\hbar) |\gamma\rangle \langle \gamma|$ on $|\Psi^e\rangle$. Noting that the population in the S_2 is given as $P_{S_2}(t) = \langle \Psi_a(t)|Q|\Psi_a(t)\rangle$, we can use Eq. (8) to obtain that

$$P_{S_2} = \frac{\epsilon_a^2}{\hbar^2} \langle \Psi^e|\gamma\rangle \langle \gamma|Q|\gamma\rangle \langle \gamma|\Psi^e\rangle = \frac{\epsilon_a^2}{\hbar^2} |\langle \gamma|\Psi^e\rangle|^2 \langle \gamma|Q|\gamma\rangle = \frac{\epsilon_a^2}{\hbar^2} |\langle \gamma|\Psi^e\rangle|^2 \left[\sum_{\kappa} |\langle \kappa|\gamma\rangle|^2 \right]. \quad (9)$$

That is, the CW-generated S_2 population is time-independent, but $|\gamma\rangle$ -dependent.

The $\sigma(E_\gamma)$ cross section of Eq. (1) can also be written as the expectation value of the single-state projector $|\gamma\rangle \langle \gamma|$ in the $\mu|g\rangle \equiv |\Psi^e\rangle$ state,

$$\sigma(E_\gamma) = \frac{4\pi^2 \omega_{\gamma,g}}{c} \langle g|\mu|\gamma\rangle \langle \gamma|\mu|g\rangle = \frac{4\pi^2 \omega_{\gamma,g}}{c} \langle \Psi^e|\gamma\rangle \langle \gamma|\Psi^e\rangle = \frac{4\pi^2 \omega_{\gamma,g}}{c} |\langle \gamma|\Psi^e\rangle|^2. \quad (10)$$

Comparing Eqs. (9) and (10) gives the following relationship between the CW-generated population at E_γ and the cross section $\sigma(E_\gamma)$:

$$P_{S_2} = \frac{\epsilon_a^2 c}{4\pi^2 \hbar^2 \omega_{\gamma,g}} \sigma(E_\gamma) \langle \gamma|Q|\gamma\rangle. \quad (11)$$

III. COMPUTATIONAL RESULTS FOR THE PYRAZINE $S_0 \rightarrow S_2/S_1$ PHOTOEXCITATION CROSS SECTION

A. Coarse-Graining of the Pyrazine Vibronic Structure

Pyrazine has 24 vibrational degrees of freedom and approximately 10^{10} $|\gamma\rangle$ states [12, 20] at ~ 2 eV above the $S_0 \rightarrow S_1$ vertical energy difference. For the computations to be numerically feasible, we replace the exact states with a set of approximate “coarse-grained” states [12]. We thus divide the energy axis into 2000 bins I_α of size Δ_α , center energy E_α and density of states ρ_α . The projector onto a coarse-grained state $|\alpha\rangle$ is defined as

$$|\alpha\rangle\langle\alpha| = (1/(\rho_\alpha\Delta_\alpha)) \sum_{\gamma \in I_\alpha} |\gamma\rangle\langle\gamma|, \quad \text{hence} \quad \sqrt{\rho_\alpha\Delta_\alpha}|\alpha\rangle\langle\alpha|\sqrt{\rho_\alpha\Delta_\alpha} = \sum_{\gamma \in I_\alpha} |\gamma\rangle\langle\gamma|.$$

Thus, the coarse-grained state $|\alpha\rangle$ effectively replaces all the $|\gamma\rangle$ states in bin I_α . Numerically, the weighted states $|\bar{\alpha}\rangle \equiv \sqrt{\rho_\alpha\Delta_\alpha}|\alpha\rangle$ and their overlaps with resonances $|\kappa\rangle$ are available through our iterative solution method for pyrazine (described in detail in Ref. [12]).

The above coarse-grained description of the pyrazine vibronic structure is fully adequate for vibronic femtosecond $S_2 \leftrightarrow S_1$ internal conversion dynamics [12, 13, 16]. It involves a manifold of 76775 $|\bar{\alpha}\rangle$ coarse-grained vibronic states, spanning the energy range of 2 eV above the $S_0 \rightarrow S_1$ vertical electronic transition. The density of $|\bar{\alpha}\rangle$ states is nonuniform with average vibronic energy separation of 2.6×10^{-5} eV = 0.21 cm⁻¹, which happens to coincide with some rotational energy spacings. Thus, if one considers vibronic $S_0 \rightarrow S_2$ excitation by a CW laser, which is narrow enough to resolve particular $|\bar{\alpha}\rangle$ states separately, one also needs to account for the rotational transitions and consider the full ro-vibronic spectrum. However, as discussed in the Appendix, if one assumes that pyrazine is initially cold, then consideration of vibronic levels only is sufficient.

To compute the cross section numerically, we thus replace $\langle\gamma|\kappa\rangle$ by $\langle\bar{\alpha}|\kappa\rangle$ and E_γ by E_α , throughout. When this is done, the cross section for the state $|\bar{\alpha}\rangle$ is given [using Eq. (1)] as

$$\sigma(E_\alpha) = \frac{4\pi^2\omega_{\alpha,g}}{c} |\langle\bar{\alpha}|\mu|g\rangle|^2 = \frac{4\pi^2\omega_{\alpha,g}}{c} \langle g|\mu|\bar{\alpha}\rangle \langle\bar{\alpha}|\mu|g\rangle = \frac{4\pi^2\omega_{\alpha,g}}{c} \langle\Psi^e|\bar{\alpha}\rangle \langle\bar{\alpha}|\Psi^e\rangle = \frac{4\pi^2\omega_{\alpha,g}}{c} |\langle\bar{\alpha}|\Psi^e\rangle|^2, \quad (12)$$

where $\omega_{\alpha,g} \equiv (E_\alpha - E_g)/\hbar$. In terms of $|\gamma\rangle$ states, this gives

$$\sigma(E_\alpha) = \sum_{\gamma \in I_\alpha} \frac{4\pi^2\omega_{\alpha,g}}{c} \langle\Psi^e|\gamma\rangle \langle\gamma|\Psi^e\rangle \approx \sum_{\gamma \in I_\alpha} \frac{4\pi^2\omega_{\gamma,g}}{c} \langle\Psi^e|\gamma\rangle \langle\gamma|\Psi^e\rangle = \sum_{\gamma \in I_\alpha} \sigma(E_\gamma). \quad (13)$$

Hence, $\sigma(E_\alpha)$ is approximately the cumulative sum of all the individual cross sections for all the $|\gamma\rangle$ in this bin I_α . This is a reasonable approximation as long as the I_α bin size is small.

As in Eq. (3), the coarse-grained cross section of Eq. (12) can be decomposed into diagonal and interference contributions,

$$\sigma^{\text{diag}}(E_\alpha) = \sum_{\kappa} \frac{4\pi^2\omega_{\alpha,g}}{c} |\langle\bar{\alpha}|\kappa\rangle \langle\kappa|\mu|g\rangle|^2 \equiv \sum_{\kappa} \sigma_{\kappa}^{\text{diag}}(E_\alpha), \quad (14)$$

and

$$\begin{aligned}\sigma^{\text{interf}}(E_\alpha) &= \sum_{\kappa \neq \kappa'} \frac{4\pi^2 \omega_{\alpha,g}}{c} \langle g|\mu|\kappa\rangle \langle \kappa'|\mu|g\rangle \langle \kappa|\bar{\alpha}\rangle \langle \bar{\alpha}|\kappa'\rangle \\ &\equiv \sum_{\kappa \neq \kappa'} \sigma_{\kappa,\kappa'}^{\text{interf}}(E_\alpha) = \sum_{\kappa < \kappa'} 2 \sigma_{\kappa,\kappa'}^{\text{interf}}(E_\alpha),\end{aligned}\quad (15)$$

respectively ($\sigma_{\kappa,\kappa'}^{\text{interf}}(E_\alpha)$ in Eq. (15) are real).

This result is analogous to that obtained earlier. That is, each pairwise interference term $\sigma_{\kappa,\kappa'}^{\text{interf}}(E_\alpha)$ in the coarse-grained case is proportional to the product $\langle \kappa|\bar{\alpha}\rangle \langle \bar{\alpha}|\kappa'\rangle$, which is non-zero only if both $\langle \kappa|\bar{\alpha}\rangle$ and $\langle \bar{\alpha}|\kappa'\rangle$ are non-zero, *i.e.*, the resonances $|\kappa\rangle$ and $|\kappa'\rangle$ overlap by means of the common coarse-grained state $|\bar{\alpha}\rangle$ [12, 16]. Only under such circumstances $\sigma_{\kappa,\kappa'}^{\text{interf}}(E_\alpha)$ is non-zero.

B. Computational Results for the $S_0 \rightarrow S_2/S_1$ Photoexcitation Cross Section

In this study, transition dipole matrix elements $\langle \kappa|\mu|g\rangle$ are approximated by the corresponding Franck-Condon factors [12]. One hundred and seventy six “brightest” $|\kappa\rangle$ resonances, having the largest Franck-Condon factors, were taken into account. These bright $|\kappa\rangle$ are numbered hereafter in order of ascending zero-order energy E_κ^0 .

The interference term in Eq. (15) can be positive or negative at any given E_α , resulting in a constructive or destructive interference contribution to the photoabsorption cross section. The latter case is of particular interest, because it can lead to interference-induced transparency in the absorption profile. As an example, we consider the neighborhood of the particular resonance $|\kappa = 94\rangle$. The diagonal term $\sigma_\kappa^{\text{diag}}(E_\alpha)$ for this resonance is shown in Fig. 1, together with the position of its zero-order energy, $E_{\kappa=94}^0 \approx 5.1342$ eV. The energy of the resonance maximum, $E_{\kappa=94}^{\text{max}} \approx 5.1350$ eV, differs from $E_{\kappa=94}^0$ by a value $\Delta_{\kappa=94} \approx 8.0 \times 10^{-4}$ eV (6.45 cm^{-1}), a resonance shift due to S_1 - S_2 vibronic nonadiabatic coupling.

For the particular energy $E_{\kappa=94}^{\text{max}}$, the contribution $\sigma_{\kappa=94}^{\text{diag}}(E_{\kappa=94}^{\text{max}})$ from the particular resonance $|\kappa = 94\rangle$ dominates the full diagonal cross section $\sigma^{\text{diag}}(E_{\kappa=94}^{\text{max}})$, with $\sigma_{\kappa=94}^{\text{diag}}(E_{\kappa=94}^{\text{max}})/\sigma^{\text{diag}}(E_{\kappa=94}^{\text{max}}) \approx 0.80$ (see Fig. 2). One expects the total cross section $\sigma(E_{\kappa=94}^{\text{max}})$ to be of the same order of magnitude, but in this particular case the total cross section $\sigma(E_{\kappa=94}^{\text{max}})$ is actually much smaller than both $\sigma^{\text{diag}}(E_{\kappa=94}^{\text{max}})$ and $\sigma_{\kappa=94}^{\text{diag}}(E_{\kappa=94}^{\text{max}})$, leading to the local transparency. This transparency is due to the large negative (destructive) interference contribution $\sigma^{\text{interf}}(E_{\kappa=94}^{\text{max}})$. The result is shown in Fig. 2. Namely, the total cross section, composed of contributions from 176 bright $|\kappa\rangle$ resonances, is 23.4 times smaller at $E = E_{\kappa=94}^{\text{max}}$ than the contribution from the one resonance $|\kappa = 94\rangle$, an effect due to overlapping $|\kappa\rangle$ resonances.

It is instructive to analyze the structure of $\sigma^{\text{diag}}(E_{\kappa=94}^{\text{max}})$ and $\sigma^{\text{interf}}(E_{\kappa=94}^{\text{max}})$. The former is composed of 176 terms $\sigma_\kappa^{\text{diag}}(E_{\kappa=94}^{\text{max}})$, shown in Fig. 3. One can see that, out of overall 176, besides $\kappa = 94$ itself, $\kappa = 40, 70, 84, 98, 102$ and 114 contribute significantly to $\sigma^{\text{diag}}(E_{\kappa=94}^{\text{max}})$. This is a generic feature of pyrazine. That is, for any bright $|\kappa\rangle$

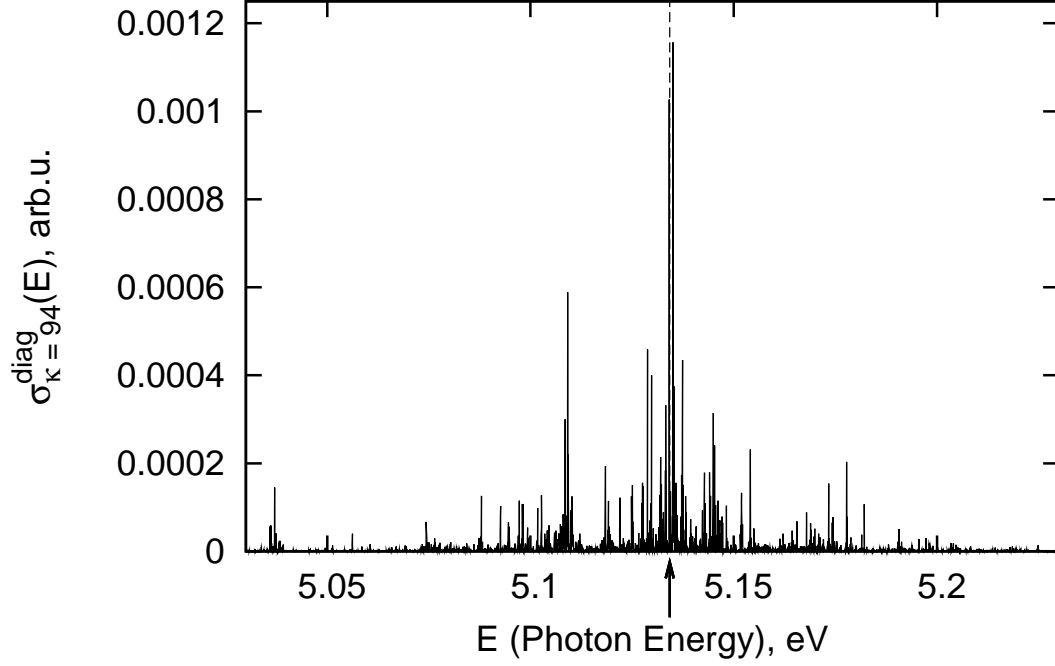


FIG. 1: Cross section contribution $\sigma_{\kappa=94}^{\text{diag}}(E)$, provided by the resonance $|\kappa = 94\rangle$. Position of $E_{\kappa=94}^0$ is shown as a vertical dashed line and an arrow on the Energy axis.

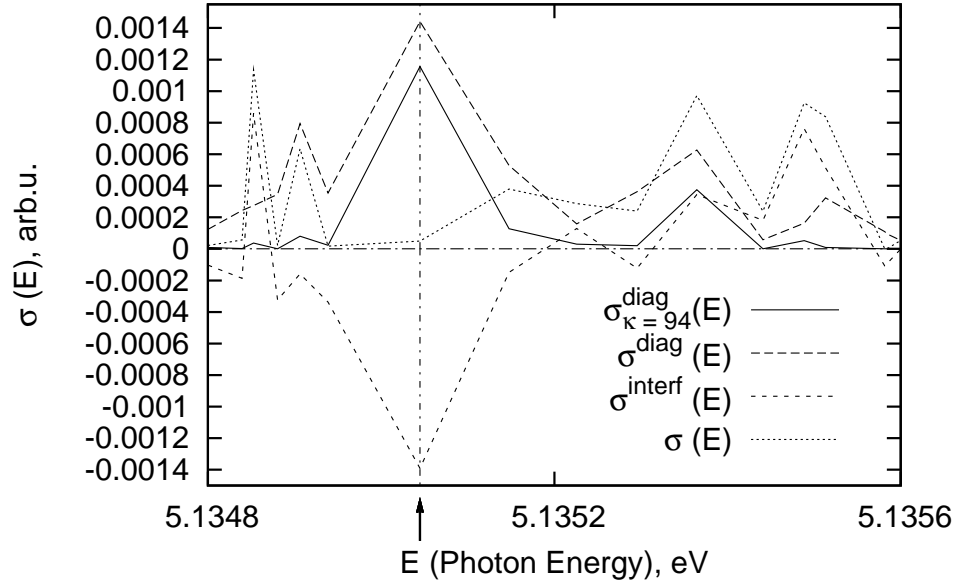


FIG. 2: Cross section contribution $\sigma_{\kappa}^{\text{diag}}(E)$ of resonance $|\kappa = 94\rangle$, together with full diagonal cross section contribution $\sigma^{\text{diag}}(E)$, full interference cross section contribution $\sigma^{\text{interf}}(E)$, and full cross section $\sigma(E)$. Position of $E_{\kappa=94}^{\text{max}}$ is shown as a vertical dash-dotted line and an arrow on the Energy axis.

only several contributions are found to be important in $\sigma_{\kappa}^{\text{diag}}(E_{\kappa}^{\text{max}})$.

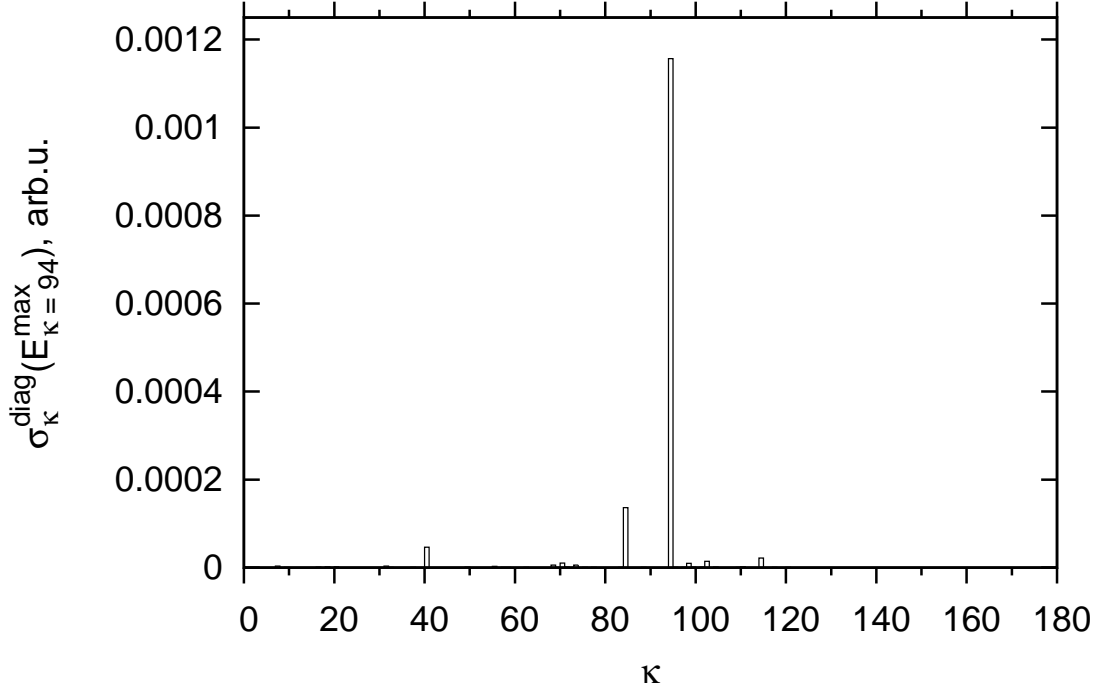


FIG. 3: Individual cross section contributions $\sigma_{\kappa}^{\text{diag}}(E)$ to $\sigma^{\text{diag}}(E)$ at $E = E_{\kappa=94}^{\text{max}}$, $\kappa = 1-176$.

For $\kappa = 1-176$, there are $176(176-1)/2 = 15400$ different pairwise interference contributions $\sigma_{\kappa, \kappa'}^{\text{interf}}(E)$ in $\sigma^{\text{interf}}(E)$. These interference contributions are presented in Fig. 4 for $E = E_{\kappa=94}^{\text{max}}$, using a one-dimensional cumulative index $\kappa + \kappa'$ ($\kappa < \kappa'$) for simplicity. The most prominent contributions to the interference part of the cross section are seen to arise from pairs of resonances with largest (by absolute value) contributions to the diagonal part (Fig. 3). Namely, the most significant pairwise interference contributions, seen in Fig. 4, are the ones with $\kappa + \kappa' = 134$ (*i.e.* $40 + 94$), 164 ($70 + 94$), 178 ($84 + 94$), 192 ($94 + 98$), 196 ($94 + 102$) and 208 ($94 + 114$). Thus, the overlap of $\kappa = 94$ resonance with these several resonances is crucial for the destructive interference causing ORIT at $E = E_{\kappa=94}^{\text{max}}$.

In addition to ORIT, the interference term in Eq. (15) can be positive, thus leading to constructive interference, amplifying the total cross section $\sigma(E)$. One characteristic example of such interference is shown in Fig. 5 for the coarse-grained vibronic state $|\bar{\alpha} = 66984\rangle$, having $E_{\alpha} = 5.704590176$ eV, for which total cross section $\sigma(E_{\alpha})$ is 10.7 times larger than the diagonal cross section term $\sigma^{\text{diag}}(E_{\alpha})$; in other words, the interference term $\sigma^{\text{interf}}(E_{\alpha})$ here is 9.7 times larger than $\sigma^{\text{diag}}(E_{\alpha})$. While in case of ORIT $|\sigma^{\text{interf}}(E_{\alpha})| \leq \sigma^{\text{diag}}(E_{\alpha})$ due to non-negativity of total cross section $\sigma(E_{\alpha}) = \sigma^{\text{diag}}(E_{\alpha}) + \sigma^{\text{interf}}(E_{\alpha})$, there is no such a limitation on the absolute value of *constructive* interference term with respect to diagonal term, as Fig. 5 shows.

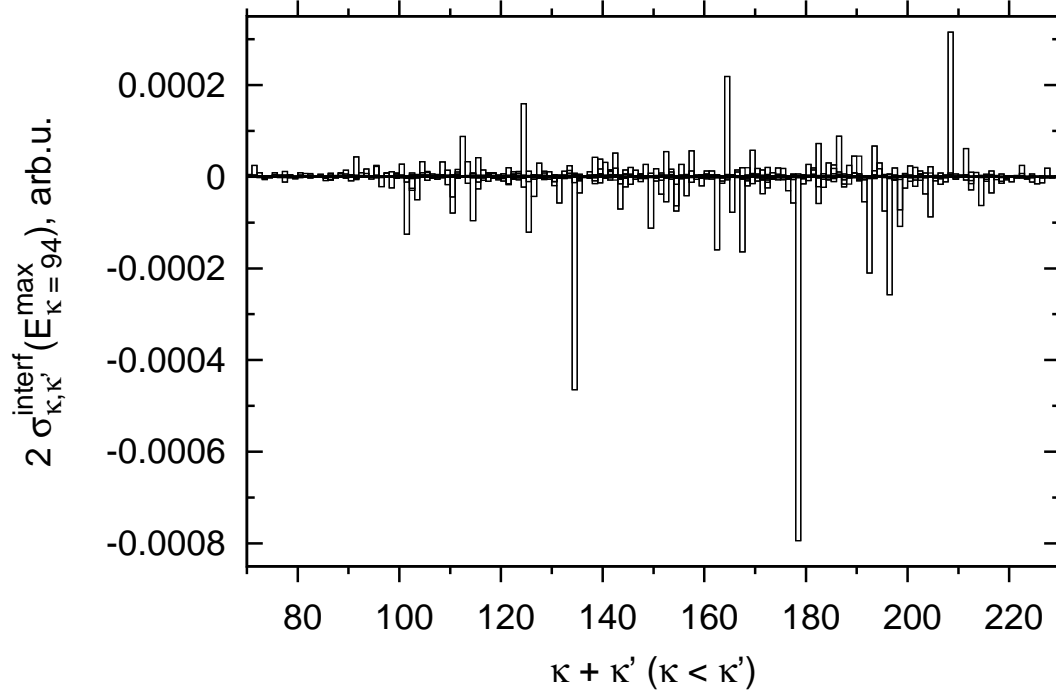


FIG. 4: Pairwise interference cross section contributions $2\sigma_{\kappa,\kappa'}^{\text{interf}}(E)$ to $\sigma^{\text{interf}}(E)$ at $E = E_{\kappa=94}^{\text{max}}$, $\kappa, \kappa' = 1-176$ ($\kappa < \kappa'$).

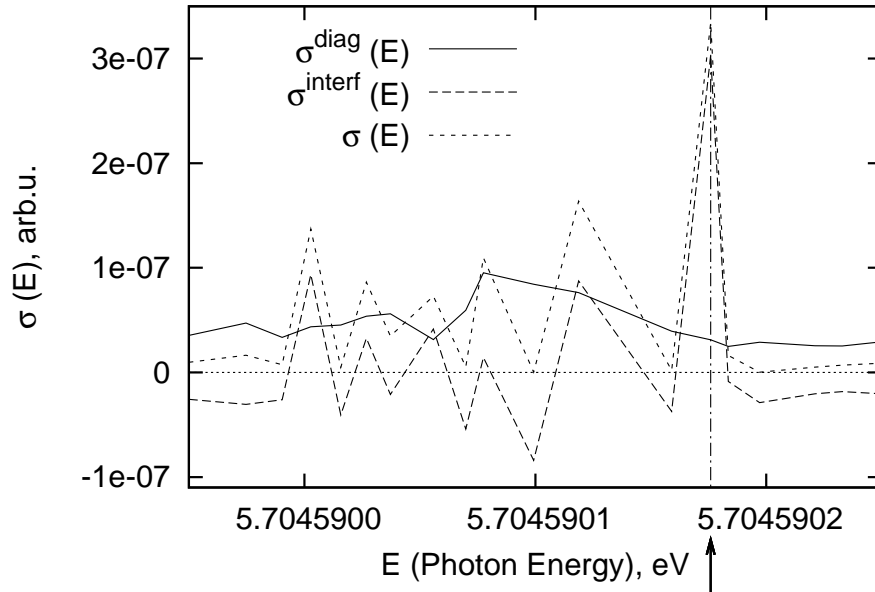


FIG. 5: Full diagonal cross section contribution $\sigma^{\text{diag}}(E)$, full interference cross section contribution $\sigma^{\text{interf}}(E)$ and full cross section $\sigma(E)$. Energy of the coarse-grained state $|\bar{\alpha} = 66984\rangle$, $E_{\alpha=66984} = 5.704590176$ eV, is shown as a vertical dash-dotted line and an arrow on the Energy axis.

IV. $S_0 \rightarrow S_2/S_1$ PHOTOEXCITATION CROSS SECTION ORIT AND CW-GENERATED S_2 POPULATION

The example of ORIT, presented and discussed above, is provided in terms of microscopic $\sigma(E)$ cross section. Physically, these effects should be observed in terms of full vibronic states $|\gamma\rangle$. However, the $S_2 \leftrightarrow S_1$ coupling, which is responsible for the very dense and rich $\sigma(E)$ structure, makes the experimental photoabsorption spectrum (obtained with finite spectral resolution and in the presence of environment) diffuse and continuous. This is the case for all pyrazine $S_0 \rightarrow S_2$ photoabsorption spectra, presented in literature [21], so that these available spectra do not allow comparison with our ORIT computation. So, instead, in this section we computationally confirm the relevance of ORIT in the cross section to the amount of CW-generated S_2 population, while the comparison with the experimental diffuse $S_0 \rightarrow S_2$ photoabsorption spectrum is presented in the next section below.

In terms of $|\bar{\alpha}\rangle$ states, the S_2 population is

$$P_{S_2}(t) = \frac{\epsilon_a^2}{\hbar^2} |\tau_\alpha(t)|^2 |\langle \bar{\alpha} | \Psi^e \rangle|^2 \langle \bar{\alpha} | Q | \bar{\alpha} \rangle, \quad (16)$$

where $\tau_\alpha(t) = \exp(-iE_\alpha t/\hbar) \sin(\Delta_\alpha t/(2\hbar))/(\Delta_\alpha t/(2\hbar))$, so that $|\tau_\alpha(t)|^2 = [\sin(\Delta_\alpha t/(2\hbar))/(\Delta_\alpha t/(2\hbar))]^2$, which tends to be ≈ 1 , if $|\Delta_\alpha t/(2\hbar)| \ll 1$, or $|t| \ll 2\hbar/\Delta_\alpha$, which is the timescale of accuracy of coarse-grained description. So, for times $|t|$ small enough, the CW-generated S_2 population is time-independent, but $|\bar{\alpha}\rangle$ -dependent, and can be written as

$$P_{S_2} = \frac{\epsilon_a^2}{\hbar^2} |\langle \bar{\alpha} | \Psi^e \rangle|^2 \langle \bar{\alpha} | Q | \bar{\alpha} \rangle, \quad (17)$$

which is fully analogous to Eq. (9) for the $|\gamma\rangle$ states.

Comparison of Eqs. (17) and (12) provides the following relationship between the CW-generated P_{S_2} and $\sigma(E_\alpha)$ using $|\bar{\alpha}\rangle$ states:

$$P_{S_2} = \frac{\epsilon_a^2 c}{4\pi^2 \hbar^2 \omega_{\alpha,g}} \sigma(E_\alpha) \langle \bar{\alpha} | Q | \bar{\alpha} \rangle, \quad (18)$$

which is similar to Eq. (11) in terms of $|\gamma\rangle$ states. The term $\langle \bar{\alpha} | Q | \bar{\alpha} \rangle = \sum_\kappa |\langle \kappa | \bar{\alpha} \rangle|^2$ in Eq. (18) is the incoherent sum, and is relatively slowly varying function of time. When $\sigma(E_\alpha)$ displays ORIT at specific energy $E = E_\alpha$ due to the destructive interference caused by the overlapping resonances, P_{S_2} is also expected to be small. This expected P_{S_2} behavior is fully confirmed computationally, using our pyrazine dynamics and control software from Ref. [16]. This serves as a “theoretical high resolution spectroscopy”, justifying the importance of the ORIT in the cross section for the computed S_2 population. As an example, the computed P_{S_2} , corresponding to the total cross section $\sigma(E)$ in Fig. 2 in the vicinity of $E = E_{\kappa=94}^{\max}$, is shown in Fig. 6. The P_{S_2} profile resembles the $\sigma(E)$ profile in Fig. 2; the distortion of P_{S_2} shape from $\sigma(E)$ shape is mostly due to the varying $\langle \bar{\alpha} | Q | \bar{\alpha} \rangle$ factor in Eq. (18).

Beyond theoretical interest, ORIT can be of practical importance for certain applications. For example, as in “EIT Spectroscopy” [22], one can selectively excite B in an A + B molecular mixture by a CW laser while leaving A

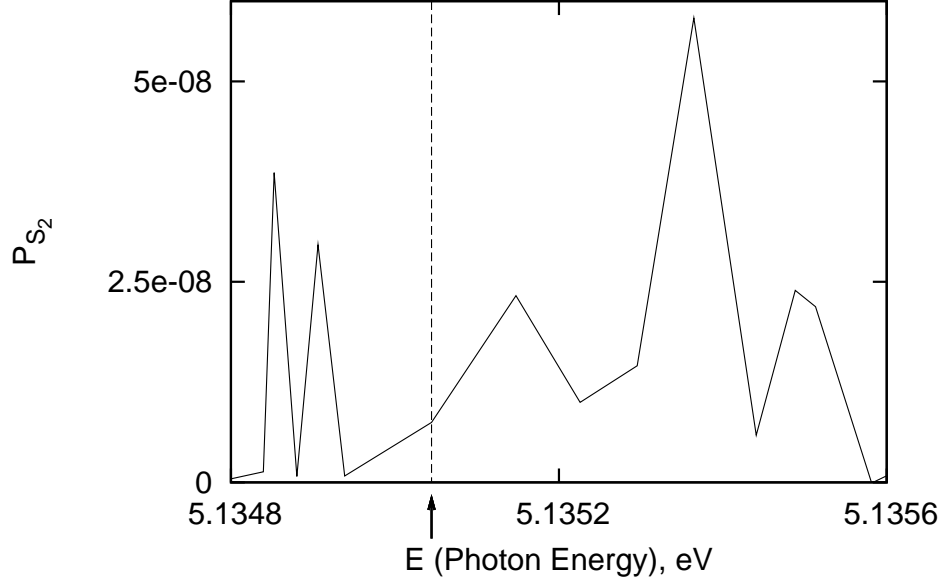


FIG. 6: CW-generated S_2 population P_{S_2} , corresponding to the total cross section $\sigma(E)$ in Fig. 2. Position of $E_{\kappa=94}^{\max}$ is shown as a vertical dash-dotted line and an arrow on the Energy axis.

in the ground state. To do so, one can use the local optical transparency of A at a certain laser frequency, when A does not absorb, provided that B absorbs well at this laser frequency.

V. COMPARISON OF THE COMPUTED $S_0 \rightarrow S_2$ PHOTOABSORPTION SPECTRUM WITH THE EXPERIMENTAL DATA

Finally, we estimate the accuracy of our pyrazine vibronic structure and associated approximations by computing the $S_0 \rightarrow S_2$ photoabsorption spectrum $I(E)$ and comparing it with the available experimental data [21]. To obtain $I(E)$, one can convolute the stick spectrum, composed of $|\langle \bar{\alpha} | \mu | g \rangle|^2$ values, with Lorentzian (as in Ref. [23]), having uniform FWHM_E in energy domain:

$$I(E) \propto \omega_{E,g} \sum_{\alpha} |\langle \bar{\alpha} | \mu | g \rangle|^2 \frac{\Gamma/2}{(\omega_{E,g} - \omega_{\alpha,g})^2 + \Gamma^2/4}, \quad (19)$$

where $\omega_{E,g} \equiv (E - E_g)/\hbar$, and $\Gamma = \text{FWHM}_E/\hbar$. Alternatively, $I(E)$ can be computed using the Fourier transform of the autocorrelation function $C(t) = \langle \Psi(0) | \Psi(t) \rangle$, where $|\Psi(0)\rangle = \mu|g\rangle = |\Psi^e\rangle$, $|\Psi(t)\rangle = U(t)|\Psi(0)\rangle = \sum_{\gamma} \exp(-iE_{\gamma}t/\hbar) |\gamma\rangle \langle \gamma | \mu | g \rangle$, thus giving $C(t) \approx \sum_{\alpha} |\langle \bar{\alpha} | \mu | g \rangle|^2 \tau_{\alpha}(t)$ in terms of coarse-grained states $|\bar{\alpha}\rangle$. Then, as in Refs. [20, 24], $I(E)$ is obtained as

$$I(E) \propto \omega_{E,g} \text{Re} \int_0^{\infty} dt \exp(-t/T_d) C(t) \exp(i\omega_{E,g}t), \quad (20)$$

where T_d is the damping parameter, giving the spectral broadening.

The spectrum $I(E)$, computed using Eq. (19) with FWHM_E of 0.05 eV, and $I(E)$, computed using Eq. (20) with $T_d = 25.0$ fs, are shown in Fig. 7 along with the experimental spectrum of Yamazaki et al. [21]. Fig. 7 shows that the overall shape of the computed spectra (which are almost identical to each other) is in very good qualitative agreement with experiment (e.g., better than in Refs. [23, 25]). Our computed spectra does lack the third peak near the maximum and somewhat overestimates absorption at low energies (before maximum), being less accurate than in Refs. [20, 24]. These quantitative differences likely reflect our use of the approximate coarse-grained $|\bar{\alpha}\rangle$ states, the simplifying restriction we impose [12] to a total of 176 S_2 bright states, and the use of a phenomenological Γ (or T_d) to describe the broadening of the S_2 states. These approximations, however, in no way affect the general physics of ORIT or of constructive spectral enhancement, which are the central focus of this paper.

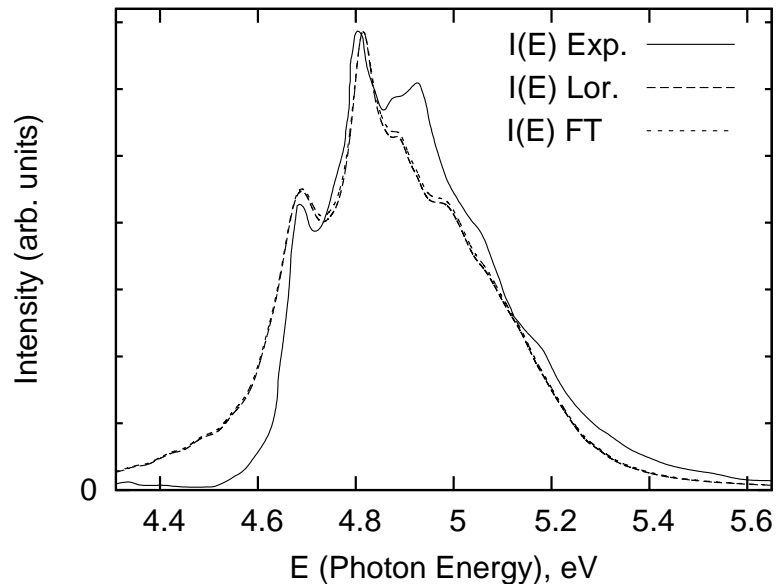


FIG. 7: Experimental pyrazine $S_0 \rightarrow S_2$ photoabsorption spectrum (full line) from Ref. [21] together with two calculated spectra (long dashed line and short dashed line). Here, $\text{FWHM}_E = 0.05$ eV, $T_d = 25.0$ fs.

VI. SUMMARY AND CONCLUSION

In conclusion, we have computationally demonstrated interference-induced transparency (and cross section enhancement) in a polyatomic molecule, using the $S_0 \rightarrow S_2/S_1$ photoabsorption cross section in pyrazine as an example. Specifically, transparency has been shown to arise from destructive quantum interferences associated with overlapping resonances [9] which are optically accessible in the $S_0 \rightarrow S_2$ photoexcitation. In the specific case examined as an example, the destructive interference between several locally important resonances was found to be responsible for the local transparency effect. Interference induced cross section enhancement was also shown. These effects are

expected to be ubiquitous in polyatomic molecules, a feature which has already been shown relevant to the coherent control of internal conversion [13, 16].

VII. ACKNOWLEDGEMENTS

The authors thank the Natural Sciences and Engineering Research Council of Canada and the NSF, under grant number CHE0848198, for funding.

Appendix: Consideration of Pyrazine Rotational Spectrum

Pyrazine is a rigid aromatic system. For low rotational angular momentum quantum numbers, one can neglect rovibrational interaction and consider the molecular Hamiltonian as a sum of rotational and vibronic parts, being independent of one another. This gives the molecular wavefunction as a product of rotational and vibronic wavefunctions, and the molecular energy as a sum of rotational and vibronic energies governed by different quantum numbers.

Pyrazine is a nearly symmetric oblate top with rotational constants $\overline{B} = (A + B)/2 \approx 0.2 \text{ cm}^{-1}$, and $C \approx 0.1 \text{ cm}^{-1}$ [26, 27]. Its rotational energy can be approximated as $E_R(J, K) = \overline{B}J(J+1) + (C - \overline{B})K^2 \approx 0.2J(J+1) - 0.1K^2 \text{ cm}^{-1}$, where J and K are rotational angular momentum and its projection on the figure axis of the top, respectively ($J \geq K$). The symmetric top rotational selection rules [28] allow only $|J'', K''\rangle \rightarrow |J', K'\rangle$ transitions, belonging to P , Q , and R branches, having $\Delta J \equiv J' - J'' = -1, 0, +1$, respectively, with $\Delta K \equiv K' - K'' = 0, \pm 1$. In case of pyrazine, belonging to the point symmetry group D_{2h} , $S_0(^1A_g) \rightarrow S_2(^1B_{2u})$ transition dipole moment belongs to B_{2u} symmetry (denoted T_y or y in the D_{2h} character table). This transition dipole moment lies in molecular plane, perpendicular to the figure axis of the top [29, 30], thus retaining only $\Delta K = \pm 1$ transitions in the $S_0 \rightarrow S_2$ rovibronic spectrum.

If the ground state is rotationally very cold, being comprised of only one lowest rotational state $|J'' = 0, K'' = 0\rangle$, then only the R branch exists. In the current case this gives only two R branch transitions $|J'' = 0, K'' = 0\rangle \rightarrow |J' = 1, K' = \pm 1\rangle$. Both transitions have relative rotational line strengths of $1/2$ [28], and the same $\Delta E_R \equiv E_R(J' = 1, K' = \pm 1) - E_R(J'' = 0, K'' = 0) \approx 0.3 \text{ cm}^{-1}$, due to rotational K -doubling. Both transitions merge into the single line in the spectrum, uniformly shifting the vibronic spectrum by $0.3 \text{ cm}^{-1} = 3.72 \times 10^{-5} \text{ eV}$, which is very small in comparison with the energy of vibronic transition, starting here from 4.06 eV , $S_0 \rightarrow S_1$ vertical electronic excitation energy [31]. Considering the rotationally very cold ground state, one indeed can focus only on vibronic transitions.

-
- [1] M. O. Scully and M. S. Zubairy, *Quantum Optics* (Cambridge University Press, UK, 1997).
- [2] M. Shapiro and P. Brumer, *Principles of the Quantum Control of Molecular Processes* (Wiley, USA, 2003); M. Shapiro and P. Brumer, *Quantum Control of Molecular Processes* (Wiley-VCH, Wertheim, 2012).
- [3] K. J. Boller, A. Imamoglu and S. E. Harris, Phys. Rev. Lett. **66**, 2593 (1991).
- [4] J. E. Field, K. H. Hahn and S. E. Harris, Phys. Rev. Lett. **67**, 3062 (1991).
- [5] S. E. Harris, Phys. Rev. Lett. **70**, 552 (1993).
- [6] S. E. Harris, J. E. Field and A. Imamoglu, Phys. Rev. Lett. **64**, 1107 (1990).
- [7] K. Ichimura, K. Yamamoto and N. Gemma, Phys. Rev. A **58**, 4116 (1998).
- [8] M. Takeoka, D. Fujishima and F. Kannari, Jpn. J. Appl. Phys. 1 **40**, 137 (2001).
- [9] M. Shapiro, J. Chem. Phys. **56**, 2582 (1972).
- [10] M. Shapiro, J. Phys. Chem. A **102**, 9570 (1998).
- [11] P. S. Christopher, M. Shapiro and P. Brumer, J. Chem. Phys. **123**, 064313 (2005).
- [12] P. S. Christopher, M. Shapiro and P. Brumer, J. Chem. Phys. **124**, 184107 (2006).
- [13] P. S. Christopher, M. Shapiro and P. Brumer, J. Chem. Phys. **125**, 124310 (2006).
- [14] I. Thanopoulos, P. Brumer and M. Shapiro, J. Chem. Phys. **133**, 154111 (2010).
- [15] I. Thanopoulos, X. Li, P. Brumer and M. Shapiro, to be published in J. Chem. Phys., 2012.
- [16] T. Grinev, M. Shapiro and P. Brumer (manuscript in preparation).
- [17] M. Tsubouchi, B. J. Whitaker and T. Suzuki, J. Phys. Chem. A **108**, 6823 (2004).
- [18] M. Shapiro, J. Phys. Chem. **97**, 7396 (1993).
- [19] R. He, C. Zhu, C.-H. Chin and S. H. Lin, Chem. Phys. Lett. **476**, 19 (2009).
- [20] A. Raab, G. A. Worth, H.-D. Meyer and L. S. Cederbaum, J. Chem. Phys. **110**, 936 (1999).
- [21] I. Suzuka, Y. Udagawa and M. Ito, Chem. Phys. Lett. **64**, 333 (1979); I. Yamazaki, T. Murao, T. Yamanaka and K. Yoshihara, Faraday Discuss. Chem. Soc. **75**, 395 (1983); A. Bolvinos, P. Tsekeris, J. Philis, E. Pantos and G. Andritsopoulos, J. Mol. Spectrosc. **103**, 240 (1984); K. K. Innes, I. G. Ross and W. R. Moomaw, J. Mol. Spectrosc. **132**, 492 (1988).
- [22] A. Eilam, E. A. Shapiro, and M. Shapiro, J. Chem. Phys. **136**, 064201 (2012).
- [23] A. K hl and W. Domcke, J. Chem. Phys. **116**, 263 (2002).
- [24] G. Stock and W. Domcke, J. Phys. Chem. **97**, 12466 (1993); M. Thoss, W. H. Miller and G. Stock, J. Chem. Phys. **112**, 10282 (2000).
- [25] R. Schneider and W. Domcke, Chem. Phys. Lett. **150**, 235 (1988).
- [26] J. A. Merritt and K. K. Innes, Spectrochim. Acta **16**, 945 (1960).
- [27] S. N. Thakur and K. K. Innes, J. Mol. Spectrosc. **52**, 130 (1974).
- [28] R. N. Zare, *Angular Momentum* (Wiley, USA, 1988).
- [29] D. M. Burland and J. Schmidt, Mol. Phys. **22**, 19 (1971).
- [30] C. Woywod, W. Domcke, A. L. Sobolewski and H.-J. Werner, J. Chem. Phys. **100**, 1400 (1994).
- [31] X. Chen and V. S. Batista, J. Chem. Phys. **125**, 124313 (2006).